

JPMTR-2109  
DOI 10.14622/JPMTR-2109  
UDC 658.5:004.352|62-5(18)

Original scientific paper | 154  
Received: 2021-08-09  
Accepted: 2021-12-03

# Designing the Spatial star as a three-dimensional derivate of the Siemens star and developing the methods to determine the accuracy, resolution and spatial frequency response from a 3D scan of the Spatial star

*Sven Ritzmann and Peter Urban*

University of Wuppertal,  
School of Electrical, Information and Media Engineering,  
Rainer-Gruenter-Straße 21, D.42119 Wuppertal

ritzmann@uni-wuppertal.de  
purban@uni-wuppertal.de

## Abstract

In many cases investigating a 3D scan of a real object is more time and cost effective than investigating the real object. This is especially the case if related objects are spread over several collections around the world. Investigation results based on a 3D scan depend on the accuracy and resolution of the specific 3D scan. This paper lays the foundation to define the specific characteristics of a workflow to determine the accuracy, resolution and spatial frequency response of any 3D scan. Therefore, it adapts the operating principle of the Siemens star to the third dimension. The result is the Spatial star, a digital three-dimensional derivate of the Siemens star that provides the required information. This paper also develops the methods to determine the accuracy, resolution and spatial frequency response from a 3D scan of the Spatial star. During this process a 3D scan is restructured into a unified matrix representation that ensures comparability between different 3D scans and fits documentation purposes. To validate the developed methods, the paper uses a set of partly simulated 3D scans of the Spatial star.

**Keywords:** 3D imaging, quality assessment, optical transfer function, modulation transfer function

## 1. Introduction

The background of this paper is a project that deals with digitization of cultural heritage items. The main purpose of the project, beneath preservation and documentation, is to ease investigations. In general, several cultural heritage items related for example in terms of era or origin are often spread over several collections all over the world. Instead of investigating related items all over the world, investigating a 3D scan of these items is less time and cost consumptive. In this case the investigation results depend on the accuracy and resolution of the investigated 3D scan. This leads to the question how the accuracy and resolution of any 3D scan can be determined to proof the relevance of such investigations.

The determination of the accuracy and resolution is of interest not only for the digitization of objects but also for the development of 3D scanning systems as well

as for the additive production of objects. Therefore, a more generalized concept was designed that is shown in Figure 1.

This concept includes three workflows for investigating 3D scanning systems (respectively 3D scans), 3D scanning algorithms and 3D printers. The first of the two key processes (filled in grey) in each workflow is a digital test element that provides information like accuracy, resolution and the spatial frequency response (SFR). The second key process determines this information from a 3D scan of the test element compared to a reference. The intervening processes vary depending on the system under test. A 3D scanning system under test digitizes a physical copy of the test element. Both the system producing the physical test element and the 3D scanning system that creates the reference must have a higher resolution capacity than the system under test. A 3D scanning algorithm under test processes a set of corresponding ground

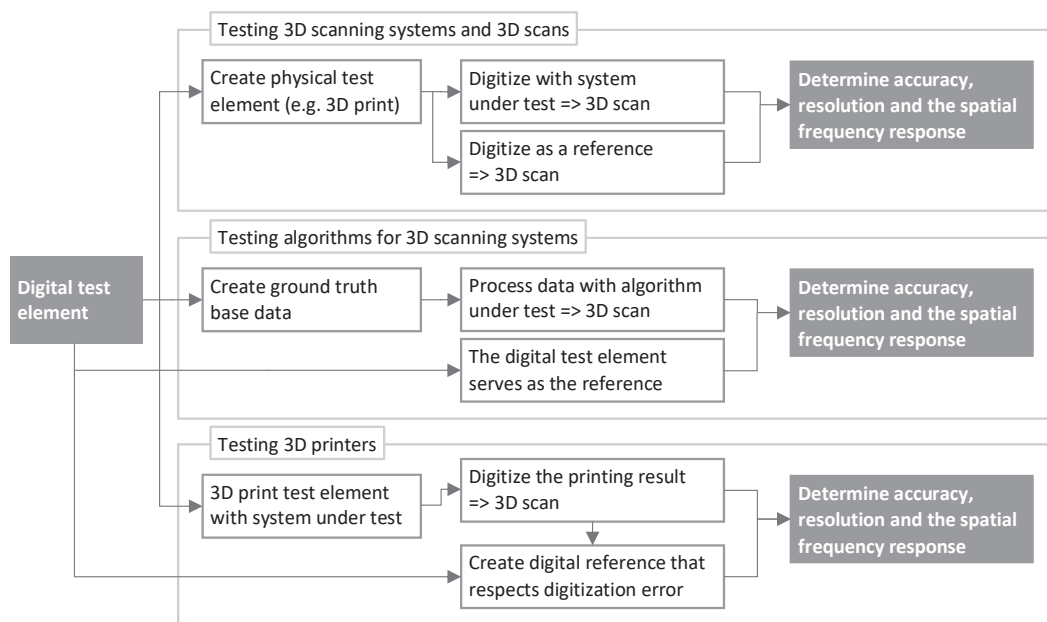


Figure 1: Three conceptual workflows to determine the accuracy, resolution and spatial frequency response of 3D scanning systems and their algorithms, 3D scans and 3D printers

truth base data created from the digital test element. In this workflow the digital test element serves as a reference without any modifications. A 3D printer under test prints the test element. A 3D scanning system with a higher resolution capacity than the system under test digitizes the printing result. To obtain the reference the digital test element is modified with respect to the digitization error of the used 3D scanning system.

The implementation of these workflows raises further questions about the characteristics of the processes. For example, to what degree the resolution capacity of a 3D scanning system has to be beyond the resolution capacity of the system under test? How to precisely produce a physical copy of the test element? How to define a ground truth dataset for several 3D scanning algorithms? Do the computed accuracy and resolution match with the human perception?

To investigate and define these characteristics and to finally implement the workflows the two key processes have to be defined in advance. Therefore, this paper introduces a digital test element that provides information like accuracy, resolution and SFR, and develops a process to determine this information from a 3D scan of the test element. Due to its importance for each workflow and for the mentioned project this paper exclusively deals with 3D scanning and neglects 3D printing.

In general, several 3D scanning systems and methods are able to digitize 3D objects and surfaces. These methods are divided in active and passive methods (Brünger, et

al., 2020). Drouin and Beraldin (2020) offer an in-depth insight into active 3D scanning methods. Simplified, these methods influence the scenery by projecting a light pattern with a known geometry (Figure 2a). Depending on its shape an object in the scene distorts the projected light pattern (Figure 2b). The comparison between the distorted and the undistorted light pattern leads to the reconstruction of the three-dimensional shape. A simple implementation of an active 3D scanning system includes a projector projecting a single line, a camera capturing the distortion of the projected line and a software reconstructing the depth information of the points along the line. To obtain a 360° reconstruction the object can be rotated along its central axis. The resulting points are stitched together to form a point cloud representation of the object.

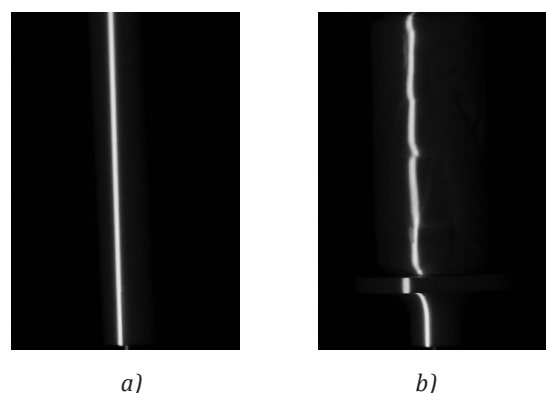


Figure 2: A line as a simple light pattern for an active 3D scanning system (a), is distorted by the shape of the 3D scanning object (b)

Contrary, passive 3D scanning methods do not influence the scene. Se and Pears (2020) offers a comprehensive description of several passive 3D scanning methods. Photogrammetry is a multi-view approach and an example for a passive 3D scanning method. A camera captures images of a scene from at least two viewpoints. A photogrammetry software detects matching features between the images (Figure 3a) and reconstructs a point in a 3D space for each feature match based on the change in perspective (Figure 3b). The resulting point cloud represents the scene. A 3D scanning system based on photogrammetry includes at least one camera and a photogrammetry software. To obtain a 360° view the relative position between the camera and scene changes after each image. Alternatively, multiple cameras are placed around the scene.

In summary most 3D scanning systems utilize at least one camera or combine a camera with a projector. The accuracy and resolution of these components can be determined by using several methods.

Despite, it is not sufficient to know the accuracy and resolution of the used components to determine the accuracy and resolution of the 3D scanning system. Besides its components different factors influence these properties.

The result of a photogrammetry scan depends, among other things, on the camera movement between each image. The accuracy of an active 3D scanning system is influenced by the relative position of the camera to the projector and by the used pattern. Furthermore, several material properties of a 3D scanning object cause problems as well (Guidi and Frischer, 2020). For example, translucent materials scatter and distort a projected light pattern or the ambient light that is needed for any camera to work. Reflective and shiny materials also cause several reconstruction errors as they distort the light.

Although it is not sufficient to know the accuracy and resolution of the components the test elements used to determine this information can be adapted to the third dimension. One of these test elements to determine the accuracy, resolution and SFR of cameras, 2D scanners and 2D printers is the Siemens star (Loebich, et al., 2007; International Organization for Standardization, 2017). This paper adapts the operating principle of the Siemens star to the third dimension. The result is the digital Spatial star that fulfills the requirements of the digital test element and thus of the first key process of the workflows shown in Figure 1.

Since the second key process compares an actual 3D scan with a reference 3D scan, the comparability between different 3D scans of Spatial stars is mandatory. As discussed before most 3D scanning methods produce a point cloud representation of an object. Ideally the points are positioned on the object surface. Between two scans, even with the same 3D scanning system, the point positions on the surface differ. Therefore, it is unlikely that a specific point in one 3D scan has a corresponding point with the same position in the other 3D scan. This paper solves the problem by restructuring the 3D scan of a Spatial star into a unified matrix representation (UMR). The development of the second key process is finished with the methods extracting the accuracy, resolution and SFR from the UMR. As the UMR includes all required information it is also used for documentation purposes.

## 2. The research approach

### 2.1 Definition of terms

As discussed in the introduction the accuracy and resolution of a 3D scanning system do not equal the accuracy and resolution of its components. It rather depends on different influencing factors that differ between different 3D scanning systems and scanning methods.

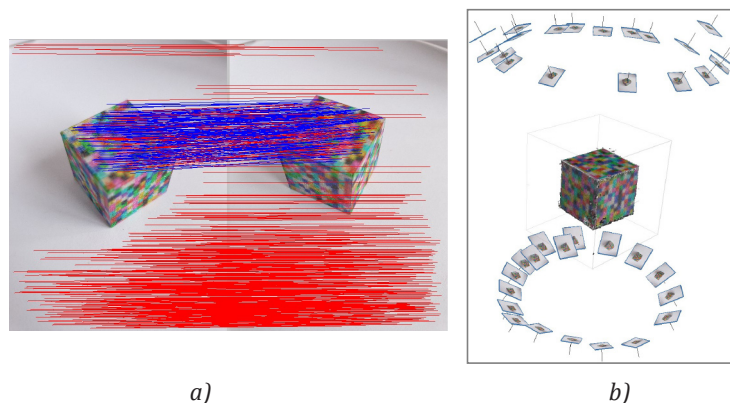


Figure 3: An example of a photogrammetry based 3D scan: the feature matches between two images are visualized with lines (a), the reconstructed object is surrounded by the reconstructed cameras (b)

To simplify the context between accuracy, resolution and influencing factors this paper refers to the combination of every influencing factor that is given by the scanning scenario as the 3D scanning system. It further refers to every influencing factor that is brought into this system as the 3D scanning object.

This paper defines a 3D scan as the result of the digitization process performed by a 3D scanning system. The accuracy of a 3D scanning system describes the maximum possible match of a reproduction and an ideal 3D scanning object where the ideal 3D scanning object has no influence on the 3D scanning system. The accuracy of a 3D scan on the other hand describes the degree a 3D scan actually matches a given 3D scanning object.

This paper describes the resolution capacity of a 3D scanning system as its ability to distinguish details. The resolution of a 3D scan is defined as the distinguishable height differences per length (later referred to as DHD value, expressed as dhd/cm).

## 2.2 The Siemens star and its operating principle

The Spatial star adapts the main operating principle from the Siemens star. The Siemens star is a 2D test chart to determine the resolution of cameras and 2D scanners. It consists of elongated triangular black spokes on a white ground arranged in a circle with a fixed angle to each other (Figure 4a). The angle is chosen so that the white space between two spokes has the same shape and size as one spoke. As the spokes get narrower towards the center the Siemens star represents (in theory) every spatial frequency between infinite and the frequency given by the outer radius. The spatial frequency is defined (Birch and Griffin, 2015) by the number of pairs of black and white spokes or cycles along the circumference of a given radius (Equation [1]).

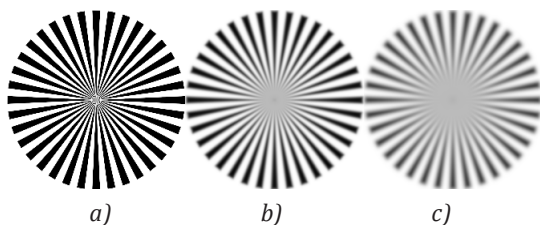


Figure 4: Three Siemens stars with 36 cycles and from the center increasing areas of no contrast due to the decreasing resolution

$$f_s = \frac{c_n}{2 \pi r} \quad [1]$$

where  $f_s$  represents spatial frequency,  $c_n$  is the number of cycles and  $r$  is the radius that corresponds to the spatial frequency.

For the increasing spatial frequency, the closer the spatial frequency is to the resolution capacity of the camera or the 2D scanner under test, the higher is the loss in contrast for the reproduction result. Spatial frequencies that exceed the resolution capacity form a circular area of no contrast around the center of the reproduced Siemens star (Figures 4b, and 4c). The radius of this area leads to the spatial frequency that corresponds to the resolution capacity of the device under test.

## 2.3 Determination of the SFR of a Siemens star

As a part of ISO 12233:2017 (International Organization for Standardization, 2017) the Siemens star is used to determine the SFR of a camera or 2D scanner. This function is a tool to analyze the contrast (respectively the response) over the spatial frequency. Loebich, et al. (2007) show how to process a reproduction of a sinusoidal Siemens star. As a part of this they determine the SFR. To compute the needed contrast, they fitted a sine function into the measurement data along the circumference of a specific radius by using the least squares method. The result is an approximation of the actual offset and amplitude that is used to calculate the contrast for the corresponding spatial frequency.

## 2.4 Determine the resolution of a Siemens star

In relation to the SFR, the resolution is the spatial frequency for a specific contrast. Perceptual wise this contrast is given by the outer radius of the area around the center of a reproduced Siemens star. To determine the resolution Loebich, et al. (2007) refer to Williams (2004 cited in Loebich, et al., 2007) who used the R10 criterion by Lord Rayleigh to define the smallest distinguishable contrast. As a result, they define the limiting resolution as the spatial frequency where the SFR reaches 10 % of the contrast. In this paper the same value is used as a comparison to the calculated DHD.

## 2.5 Preference of the Siemens star over the slanted edge method

While the Siemens star is a sine-based method for SFR measurement, the ISO 12233:2017 (International Organization for Standardization, 2017) also refers to an edge-based SFR measurement. Here the system under test captures a slanted edge. The transition in intensity from the edge to the background leads to the edge spread function which shows the pixel intensity over the pixel position. The derivative of the edge spread function is the line spread function. To obtain the SFR the line spread function is transferred into the Fourier domain (Masaoka, 2018). Goesele, Fuchs and Seidel (2003) transferred the slanted edge method into the third dimension to determine the SFR of laser scanners.

Due to two reasons this paper prefers the Siemens star as a starting point. Firstly, contrary to the slanted edge method the Siemens star allows a visual interpretation. Secondly, most 3D scanners rely on motion to achieve a 360° view. Therefore, the test element has to cover angle dependencies. Contrary to the slanted edge the circular arrangement of the Siemens star covers a wide range of angles. Furthermore, every spoke of the Siemens star (and of the Spatial star) can be seen as a slanted edge with which it keeps the possibility to implement the slanted edge method.

## 2.6 Used software and frameworks

The Spatial star is designed in OpenSCAD version 2021.01 (Kintel, 2021). The Spatial star processing and visualization software (SSPV) is written in Python and uses different frameworks like NumPy version 1.19.2 (Harris, et al., 2020) and SciPy version 1.6.1 (Virtanen, et al., 2020) for scientific computing, Pandas version 1.2.1 (McKinney, 2010) for data analysis and processing, Open3D version 0.11.2 (Zhou, Park and Koltun, 2018) for handling 3D files and Matplotlib version 3.3.2 (Hunter, 2007) for creating visualizations. Furthermore, Blender version 2.92.0 (Blender Online Community, 2021) is used to visualize the digital Spatial star and the 3D scans. Blender is also used for simulation purposes. For testing purposes, the standard edition of the photogrammetry software Metashape version 1.7.3 (Agisoft, 2021a), CloudCompare version 2.11 alpha (CloudCompare, 2021) and ExifTool version 12.32 (Harvey, 2021) are used. Cloud Compare is also used to visualize point clouds.

## 2.7 Creating sample data for visualization and validation purposes

The design of the digital Spatial star and the methods to determine the accuracy, resolution and SFR from any 3D scan of a Spatial star are described in general terms in section 2.8 and 2.9. Despite the general description, most of the figures and the validation in section 3 are based on partly simulated 3D scans of a digital Spatial star with a defined geometry.

Figure 5 visualizes the dimensions of the digital Spatial star used. It shows a top view of the star like arrangement (top left) of 30 elements, with four points per element, a radius of 25 mm and a height of 5.24 mm. For a better overview it is excluded from the outer body (top center). For orientation and alignment purposes the outer body has a cut-out mark on its left side. The fusion of both forms the digital Spatial star used in this paper (top right). Due to the fusion and the slope on the inside of the outer body, the maximal element height (height difference) of 3.83 mm is given by  $r_{max,hd}$  with 18.26 mm (Figure 5). The bottom row shows a side view of the star like arrangement (left) and of a section through the outer body (right). The white lines visualize the terms element (1), cycle (2), and element width (3) which equals the element height (4). The digital Spatial star is programmed in OpenSCAD. The parameters of the Spatial star are adaptable variables. The digital Spatial star is saved as STL file that describes an object with triangular areas each defined by three points (Kai, Jacob and Mei, 1997). Since the relevant points of the star like arrangement are set and

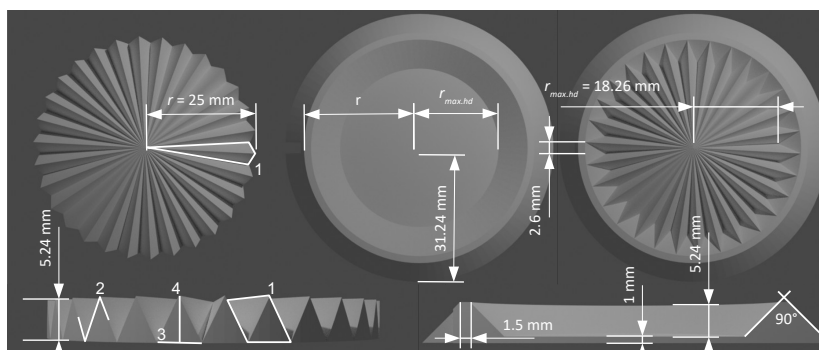


Figure 5: The dimensions of the digital Spatial star and the related terms: element (1), cycle (2), element width (3) and element height (4) as used in this paper

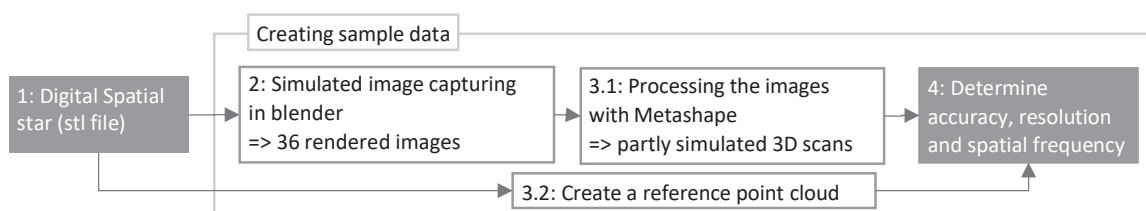


Figure 6: The workflow for creating sample data

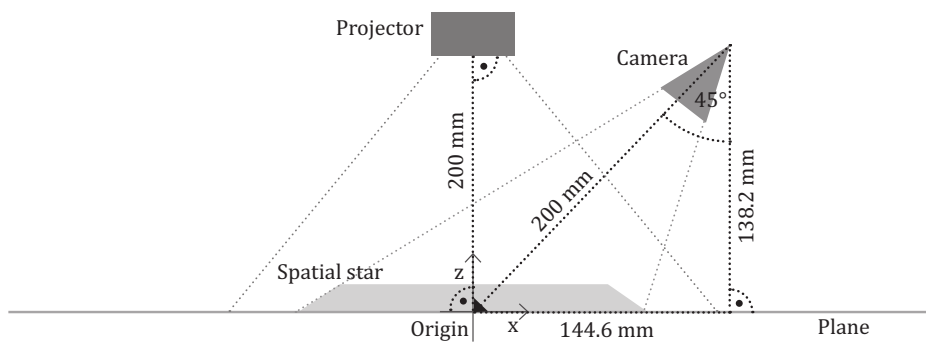


Figure 7: The arrangement in Blender to simulate the image capturing

connected to triangles as described in section 2.8 the accuracy of the digital Spatial star equals the accuracy of a double floating-point number.

The digital Spatial star is the starting point of the workflow for creating sample data as shown in Figure 6. The processes 2 and 3.1 represent a photogrammetry based 3D scanning system. While the processing is performed in Metashape as for a real set of images the preceding image capturing is simulated in Blender.

Figure 7 visualizes the arrangement used in Blender. In this scenario the digital Spatial star is the 3D scanning object. The color of the digital Spatial star is white ( $R=G=B=1.0$ ) and its surface is set to the parameter diffuse bidirectional scattering distribution function (BSDF). Its bottom center is placed at the origin. The 3D scanning system includes the camera, the projector and a plane. The plane has the same surface and color as the digital Spatial star and serves as a base.

The simulated camera captures images with a size of  $6000 \times 4000$  px. The focal length is set to 100 mm and the F-Stop value is set to 128.0. For the other camera settings, the default values remain unchanged. During the capturing process, the camera rotates 10 degrees around the z-axis after each image. The images are rendered to disk using the cycles renderer with the default settings. The projector projects an image that shows gray scaled pixel noise with a Gaussian distribution onto the digital Spatial star to create a high number of features. Therefore, the projector is not used as for an active 3D scanning method. During the image capturing, the projector remains static.

Figure 8 shows one of the 36 images of the digital Spatial star created during the simulated capturing process. These images are lacking meta data. Since Metashape uses metadata such as focal length and sensor pixel size for its internal processes (Agisoft, 2021b) these data have to be added. Therefore, ExifTool is used to copy the meta data from a reference image to each of the simulated images. The reference image is captured

using a Canon Eos 750d (Canon Deutschland GmbH, 2021) with the same focal length and image size as the simulated camera.

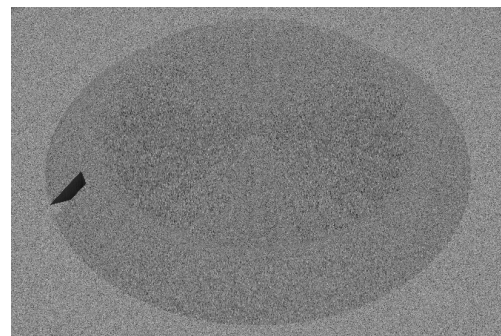


Figure 8: One of the 36 simulated images of the Spatial star

Metashape processes these images into a point cloud representation and thus into a 3D scan of the Spatial star. To obtain four 3D scans the quality parameter for the dense cloud processing is switched between high, medium, low and lowest. This scales the images to the size of  $3000 \times 2000$  px for high,  $1500 \times 1000$  px for medium,  $750 \times 500$  px for low and  $375 \times 250$  px for lowest. As defined in section 2.1, this procedure corresponds to using four 3D scanning systems. The parameter depth filtering is set to aggressive. For the other settings the default values remain unchanged. The four resulting partly simulated 3D scans are saved as a ply file. Points outside the reconstructed Spatial star are removed.

The reference point cloud mentioned in process 3.2 (Figure 6) is calculated in Cloud Compare. The function sample point cloud on mesh distributes 10 million points on the surface of the digital Spatial star. This reference point cloud is also saved as a ply file.

The software described in section 2.9 processes the partly simulated 3D scans and the reference point cloud to determine the accuracy, resolution and SFR. The discretization step length (STP) for computing the UMR (section 2.9.1) is set to 0.025 mm and is only

changed to show the influence of different values on the SFR (section 3). The non-tolerable error (NTE) for computing the accuracy UMR (section 2.9.4) is set to 0.05 mm and is twice as high as the STP value. This value is chosen arbitrarily as the STP value is determined by the requirements of the specific use case.

The discrete reference cross section used in sections 2.9.1 and 2.9.3 is calculated using Equations [2] to [14] with a radius of 18.26 mm, 30 elements, 4 points per element and a discretization step of 0.025 mm.

The figures in section 2 are exemplary and use the partly simulated 3D scan generated in Metashape with the medium quality parameter (Figures 11, 12, 18, 19, 20, 21), the reference point cloud (Figures 13, 14, 15, 17) and the discrete reference cross section (Figures 10, 12, 19).

## 2.8 Design of the Spatial star

The Spatial star is a digital 3D derivate of the Siemens star. The requirements influencing the designing process and the transformation from a planar graphical element to the 3D specimen exemplary shown in Figure 9 are discussed as well as the way a 3D scanning system distorts the Spatial star.

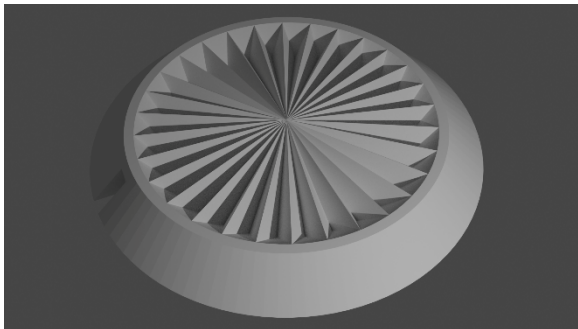


Figure 9: Example of a Spatial star with 30 cycles

The Spatial star is a crucial part to determine the accuracy and SFR of any 3D scanning system and 3D scan. Therefore, its structure has to provide this information and has to be compatible with a wide range of 3D scanning systems. Strongly simplified every 3D scanning system measures the distance to the scene points based on at least two known positions defined by its main components. Depending on the used method these components are at least one camera or one camera and one projector. Correspondingly, the surface of the Spatial star has to be completely visible to both kind of devices.

As a digital derivate of the Siemens star the Spatial star has to adapt its operating principle. Therefore, its structure has to represent an increasing spatial resolution towards its center.

Since most 3D scanning systems rely on motion to achieve a 360° view of a scene the motion path influences the 3D scan. Therefore, the Spatial star has to represent the influence of the relative position between the motion path and a structure element.

These requirements lead to the structure of the Spatial star. Its main part is a circle consisting of elements getting narrower towards the center. This is a similar layout to the Siemens star. To achieve spatiality the elements are based on a sine function. The sine function is applied perpendicular along the circumference of a circle. Every cycle proceeds along a definable number of data points. The height of one element is the same as its width. These descriptions are represented by Equations [2] to [4]:

$$p_i = \begin{pmatrix} p_x \\ p_y \\ p_z \end{pmatrix} = \begin{pmatrix} r \times \sin\left(360 \times \frac{i}{p_n}\right) \\ r \times \cos\left(360 \times \frac{i}{p_n}\right) \\ h \times 0.5 \times \left(\sin\left(360 \times e_n \times \frac{i}{p_n}\right) + 1\right) \end{pmatrix} \quad [2]$$

with  $i = \{1, \dots, p_n\}$

$$h = \frac{2 \pi r}{e_n} \quad [3]$$

$$p_n = e_n \times p_{n,\text{data}} \quad [4]$$

with  $p_{n,\text{data}} = \{x | x \geq 2 \times k\}$

with  $k = \{2, 3, \dots\}$

where  $p_i$  is the  $i$ -th point along the circumference defined by  $p_x, p_y, p_z$ ;  $r$  is the radius,  $h$  is the height for each element at radius  $r$ ,  $e_n$  is the number of elements,  $p_n$  is the number of points along the circumference, and  $p_{n,\text{data}}$  is the number of data points per element.

To represent increasing spatial frequencies each two consecutive points along the sine function form a triangular area with the center point  $p_c$ . The height of  $p_c$  is given by the outer radius and Equation [3]. Therefore, the highest point of the circumferential cross section of each radius lies in the same plane. As the radius decreases the element width and height also decreases, while the spatial frequency increases.

As a result, for each radius the circumferential cross section has the same shape, but differs in length and height. The shape approximates the sine function to a degree defined by  $p_{n,\text{data}}$ . In this paper  $p_{n,\text{data}}$  equals four to adapt the operating principle of the Siemens star (see section 2.8.1). This leads to a triangular shaped circumferential cross section as in an example shown in Figure 10.

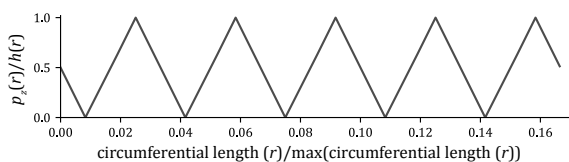


Figure 10: A Portion of the ideal circumferential cross section

Consequently, each radius corresponds to DHD as shown in Equation [5]. The DHD value defines the 3D resolution of a 3D scan. Its reciprocal value indicates the spatial dimension of the smallest detail.

$$DHD = \frac{1}{h} \tag{5}$$

Furthermore, every relevant point of the Spatial star can be seen by a camera or projector with a perpendicular view from above. This complies the compatibility with a wide range of 3D scanning systems. Due to the circular arrangement each element meets a linear motion path in a different angle. This is sufficient to represent the influence of the relative position of the 3D scanning object to the motion path.

Finally, the star like arrangement of the Spatial star is surrounded by an outer body as in an exemple shown in section 2.7.

### 2.8.1 Adapting the operating principle of the Siemens star

Depending on its resolution capacity a 3D scanning system distorts the ideal Spatial star. The distortion rounds off the corners of the triangular shaped circumferential cross sections. This effect is used to adapt the operating principle of the Siemens star.

The spatial frequencies that exceed the resolution capacity of a 3D scanning system form a circular area around the center of the reproduced Spatial star (an exemple shown in Figure 11).

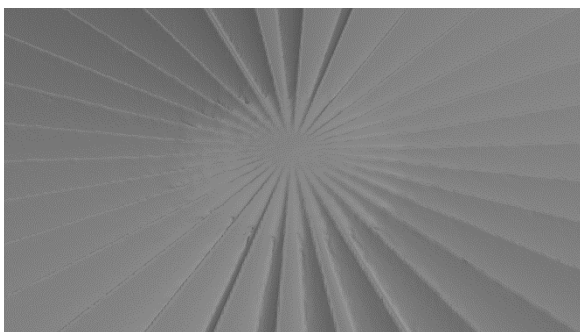


Figure 11: The circular area around the center of a partly simulated 3D scan of the Spatial star

This behavior is the same as for the Siemens star and therefore expected and desired. Equivalent to the Siemens star the outer radius of this circular area corresponds to the first radius that distinguishes the correct number of height differences. The DHD value of a 3D scan is calculated with this radius.

Contrary to the Siemens star a 3D scanning system distorts the corners of the circumferential cross sections of the Spatial star. Every upper and lower corner is, in theory, an ideal sharp tip. A 3D scanning system rounds off the part of a corner that exceeds its resolution capacity. The ratio of this part to the corner increases with the spatial frequency. If this part completely occupies the corner, the 3D scanning system is not able to reproduce the corresponding height difference. Figure 12 shows the circumferential cross section for two radii of the same partly simulated 3D scan to visualize this effect.

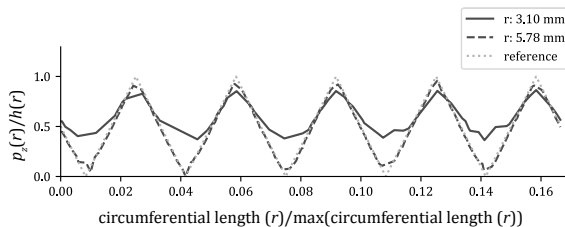


Figure 12: The corners of different circumferential cross sections of a partly simulated 3D scan in comparison

In summary the Spatial star represents the resolution of a 3D scan independently of the spatial direction. Its structure utilizes the system specific rounding off of corners in analogy to the operating principle of the Siemens star.

### 2.9 Processing a 3D scan of the Spatial star

To process the information of a 3D scanned Spatial star and thus to implement the second key process the SSPV is developed. Its first purpose is to restructure the information of a 3D scan of the Spatial star into a UMR. Its second purpose is to determine the accuracy, resolution and SFR based on the UMR.

#### 2.9.1 The unified matrix representation of a 3D scan of the Spatial star

The UMR ensures the comparability between different 3D scans of Spatial stars with the same number of elements while preserving all required information. To create the UMR the SSPV processes point clouds. For most 3D scanning systems point clouds are the raw scanning result whereas triangle meshes include further computations and algorithms.

In preparation of the UMR creation process, a 3D scan of the Spatial star has to be scaled to the size of its template. Orientation-wise it has to lie on its bottom. The star like arrangement has to face up in positive  $z$  direction. The mark in the frame has to point to the negative  $x$  direction.

To create the UMR, SSPV needs information about the 3D scanned Spatial star. This includes the maximum height difference and the corresponding radius as well as the number of elements. Another needed parameter is the discretization step length STP as SSPV unified the information by discretizing the radii and circumferential length. The actual processing is initiated by transforming each point of the 3D scan as shown in Equations [6] to [9].

$$p_{\text{transformed}} = \quad [6]$$

$$\begin{pmatrix} p_x \times \sin(-\alpha) + p_y \times \cos(-\alpha) + \alpha \times N_{xy} \times s_x \\ p_x \times \cos(-\alpha) - p_y \times \sin(-\alpha) \\ p_z \times s_z \end{pmatrix}$$

$$\alpha = \arctan2(p_y, p_x) \quad [7]$$

$$N_{xy} = \sqrt{p_x^2 + p_y^2} \quad [8]$$

$$s_x = s_z = \frac{r_{\text{max.hd}}}{N_{xy}} \quad [9]$$

where  $p_{\text{transformed}}$  corresponds to the point defined by  $(x,y,z)$  after transformation;  $\alpha$  is the angle between a point projected on the  $xy$  plane  $p(x,y)$  and  $p(1,0)$  [rad];  $p$  corresponds to a point  $p(x,y,z)$  as a part of the point cloud;  $s_i$  is scaling factor in  $i$  direction;  $N_{xy}$  is the Euclidean norm of any point  $p(x,y)$ ; and  $r_{\text{max.hd}}$  is the radius that corresponds to the maximum height difference.

While Figure 13 shows a top view of a partly simulated 3D scan, Figure 14 visualizes its transformation by Equation [6] without scaling ( $s_x = s_z = 1$ ). Due to the transformation each point on a specific circumference now lies on a straight line. Figure 15 shows the transformation by Equation [6] with  $s_x$  and  $s_z$  calculated by Equation [9]. As a result, the linearized circumferential length is the same for each radius, while the height of each point is normalized to the height given by  $r_{\text{max.hd}}$ .

As SSPV uses depth maps the height is represented by gray scales, where white represents the highest and black the lowest point. It has to be mentioned that areas with no points are also black. For orientation purposes the visualizations in Figures 13 to 15 are subdivided in eight areas that are delimited by dashed lines.

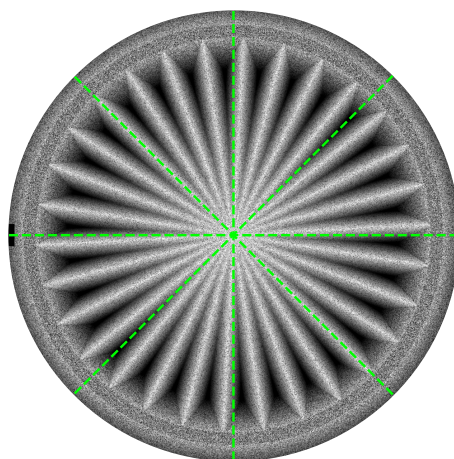


Figure 13: Top view with grey scaled height of a partly simulated 3D scan of the Spatial star

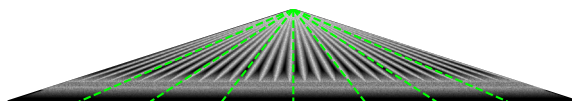


Figure 14: The points of a partly simulated 3D scan of the Spatial star transformed by Equation [6] with  $s_x = s_z = 1$

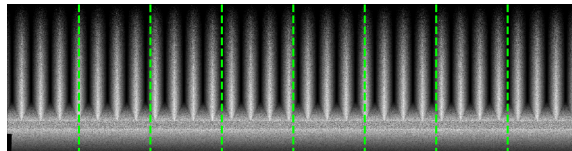


Figure 15: The points of a partly simulated 3D scan of the Spatial star transformed by Equation [6] with  $s_x$  and  $s_z$  calculated by Equation [9]

Due to the transformation the radius corresponds to the  $y$  coordinate while the circumferential length corresponds to the  $x$  coordinate and the height corresponds to the  $z$  coordinate of a transformed point. The transformation process simplifies the circumferential cross sections of a 3D scan of the Spatial star to linear cross sections and eases further calculations and processes. The scaling allows a direct comparison of circumferential cross sections with originally different length and height.

For a point cloud it is unlikely to have a sufficient number of points that lie exactly on a specific radius and circumferential length. To ensure a point-by-point comparison between different cross sections and 3D scans, SSPV implements the discretization process. The process shifts every transformed point to a specific discrete radius and circumferential length given by a multiple of discretization step length STP (Equation [10]). The `ceil` function of NumPy is used since it is less

time consuming than the round function. However, the `ceil` function causes a larger shifting error. This shifting error affects the point height. Due to the scaling process each radius has the same height difference, so that the radius shift has no effect. The circumferential shift on the other hand translates a point along the cross section in positive  $x$  direction. This shift causes when considering Equation [3] a maximum error in height that is two times the STP value. The SSPV adjusts the point height by utilizing a discrete ideal reference cross section (Equations [10] to [14]). Figure 16 visualizes the shifting, the shifting error and the adjustment.

$$p_d = \begin{pmatrix} \text{ceil}\left(\frac{p_{\text{transformed},x}}{\text{STP}}\right) \\ \text{ceil}\left(\frac{p_{\text{transformed},y}}{\text{STP}}\right) \\ p_{\text{transformed},z} * S_{z,\text{CL}} \end{pmatrix} \quad [10]$$

$$\text{CL} = \frac{p_{\text{transformed},x}}{\text{STP}} \quad [11]$$

$$S_{z,\text{CL}} = \frac{h_{\text{ref}}(\text{CL}_{\text{ceil}})}{h_{\text{ref}}(\text{CL})} \quad [12]$$

$$\text{SLP} = h_{\text{ref}}(\text{CL}_{\text{ceil}}) - h_{\text{ref}}(\text{CL}_{\text{floor}}) \quad [13]$$

$$h_{\text{ref}}(\text{CL}) = \begin{cases} (\text{CL} - \text{CL}_{\text{floor}}) \times |\text{SLP}| + h_{\text{ref}}(\text{CL}_{\text{floor}}) & \text{if } \text{SLP} \geq 0 \\ (\text{CL}_{\text{ceil}} - \text{CL}) \times |\text{SLP}| + h_{\text{ref}}(\text{CL}_{\text{ceil}}) & \text{if } \text{SLP} < 0 \end{cases} \quad [14]$$

where  $p_d$  is a point with discretized radius and circumferential length;  $p_{\text{transformed}}$  is calculated according to Equation [6];  $S_{z,\text{CL}}$  is transformation factor to correct the circumferential length shifting error;  $h_{\text{ref}}(x)$  is discrete reference cross section height at circumferential length  $x$ ;  $\text{CL}$  is circumferential length,  $\text{CL}_{\text{floor}}$  and  $\text{CL}_{\text{ceil}}$  depicted circumferential length floored or ceiled; and  $\text{SLP}$  is slope.

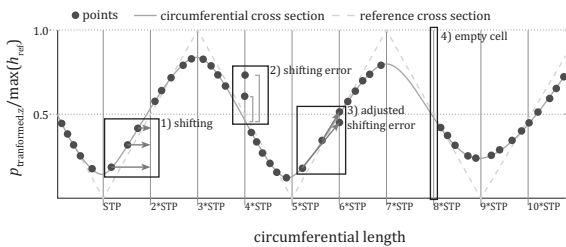


Figure 16: Visualization of the shifting (1), the shifting error (2), the adjusted shifting error (3) and empty cells (4)

The result of transforming, scaling and discretizing the point cloud is a matrix. Each matrix row represents a discrete radius (given by a number of row  $\times$  STP), while each column stands for a discrete length (given

by a number of column  $\times$  STP) on the scaled circumference. The matrix cells hold the mean value of the height of every point shifted to the corresponding row and column. As the cross sections decrease in length and height towards the center smaller radii tend to be represented by less points. The scaling spreads those points over a longer distance. As a consequence, the matrix has empty cells (4 in Figure 16). SSPV fills these empty cells by using linear interpolation (Figure 17).

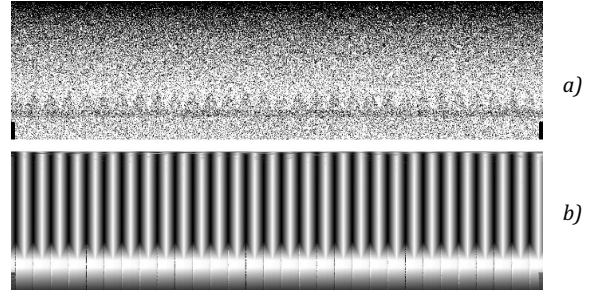


Figure 17: Visualization of empty cells (black) between the data points (white) (a), and the corresponding depth map after interpolating the empty cells (b)

After the interpolation the matrix gathers all required information provided by the 3D scan. This matrix is the UMR of a 3D scan of the Spatial star. The advantage of this representation is the point-by-point comparability between different 3D scans of Spatial stars with the same parameters.

### 2.9.2 Determining the distinguishable height differences of a 3D scan

Figure 18 visualizes the UMR of a partly simulated 3D scan. The area of low contrast at the top of the UMR represents the circular area of spatial frequencies that exceed the resolution capacity of the 3D scanning system. The first row with a visible alternating change in gray tones corresponds to the radius whose circumferential cross section distinguishes the correct number of elements.

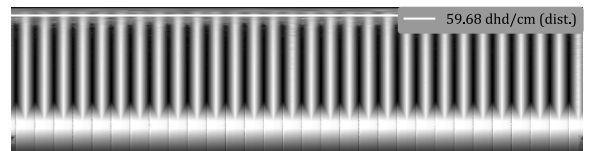


Figure 18: Visualization of the unified matrix representation of a partly simulated 3D scan (the line marks the first row that distinguishes the correct number of height differences)

To determine this row the SSPV utilizes the median function, translation and counting. For every matrix row SSPV calculates the median of the corresponding cells. The median is translated to the median of a dis-

cretized reference circumferential cross section. As a result, each cross section has the same baseline. The SSPV counts the changes around the baseline and compares the result to the number of elements of the used Spatial star. The first row with the correct number of changes corresponds to the radius of interest. The DHD are calculated as shown in Equation 5.

### 2.9.3 Determining the spatial frequency response

As discussed before, the determined value of the DHD reduces the resolution of a 3D scan to a single value. In comparison, the SFR is a more analytical approach. In the case of the Siemens star the SFR shows the contrast over the spatial frequency. For a 3D scan of the Spatial star the spatial frequency corresponds to the DHD value while the contrast corresponds to the reproduced height. Due to the scaling in height the theoretical height of the UMR is as the theoretical contrast of the Siemens star the same for each radius. Accordingly, the SSPV has to determine the actual reproduced height for each radius to determine the SFR.

$$f_{opt} = CS_{ref} \times s - CS_{actual} \tag{15}$$

where  $f_{opt}$  is a function to optimize,  $CS_{ref}$  is reference cross section,  $CS_{actual}$  is measured cross section, and  $s$  is scaling factor.

Therefore, SSPV simplifies the method shown by Loebich, et al. (2007) (see section 2.3) and uses a discretized reference cross section and a scaling factor instead of a sine function. The baselines of the reference and the measured cross section are shifted to zero by subtracting the respective median. To determine the reproduced height the SciPy function `leastsq()` optimizes the function given by Equation 15.

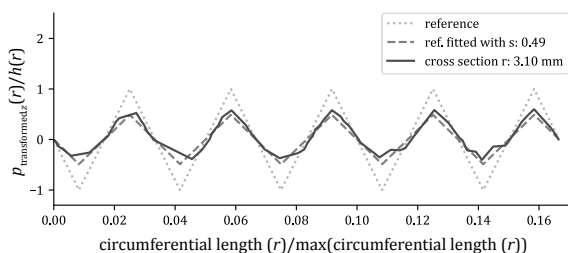


Figure 19: The reference height is fitted to the height of a cross section

Due to the shifting the only optimizable variable  $s$  scales the reference in height (Figure 19). The optimized  $s$  value corresponds to the relative reproduced height difference for the specific radius. The SSPV repeats the process for each radius and plots the reproduced height difference over the corresponding DHD value. Figure 20 shows an example of an SFR of a partly simulated 3D scan.

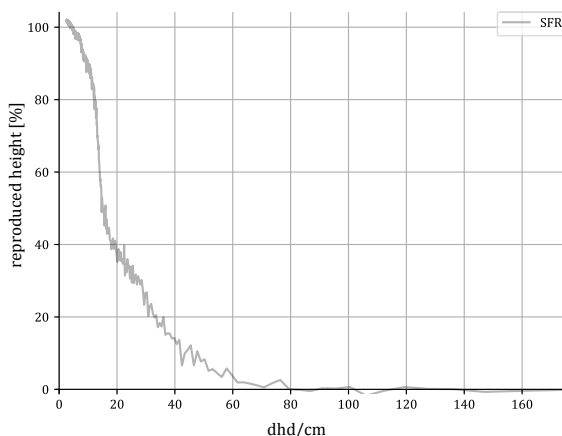


Figure 20: SFR of a partly simulated 3D scan of the Spatial star (DHD values over 160 dhd/cm are cut off due to the lack of changes)

### 2.9.4 Determining the accuracy unified matrix representation

In addition to the value of the DHD and the SFR, the SSPV determines the accuracy for each point of the UMR. The accuracy describes the degree a 3D scan matches the 3D scanning object (see section 2.1). Thus, it is the result of comparing a sample with its reference. To quantify this comparison SSPV computes the Euclidean distance between each sample point and its corresponding reference point.

Initially, the SSPV computes the UMR for both a sample point cloud and a corresponding reference point cloud. Contrary to the process described in section 2.9.1, the height is not scaled during the transformation (Equation [6] with  $s_z = 1$ ) as scaling would falsify the accuracy test. Due to the discretization process, each reference point has the same radius and circumferential length as its corresponding sample point. Therefore, the Euclidean distance is reduced to the absolute difference in height as shown in Equation [16].

$$dis_{Eucl.} = |h_{sam.} - h_{ref.}| \tag{16}$$

where  $dis_{Eucl.}$  is Euclidean distance, and  $h_{sam.}$  is height of the sample.

The SSPV calculates the Euclidean distance for each cell. The result is an accuracy UMR with the same shape as the compared UMRs. A cell value of zero defines a perfect match between the sample and the reference. A higher value means a higher loss in accuracy. The median of all accuracy values reduces the accuracy UMR to a single indicator.

To visualize the accuracy UMR, SSPV uses a color gradient. The gradient is scaled from an accuracy error of

zero to a definable NTE. Since this error depends on the requirements of the use case it cannot be universally determined. The gradient starts with green ( $dis_{Eucl.} = 0$ ) over yellow ( $dis_{Eucl.} = 0.5 \times NTE$ ) to red ( $dis_{Eucl.} \geq NTE$ ) as shown in Figure 21.

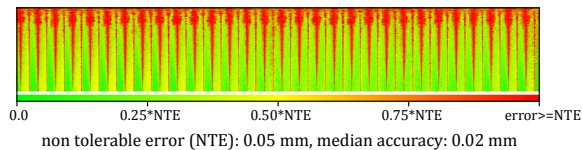


Figure 21: The accuracy UMR of a partly simulated 3D scan with an arbitrarily chosen NTE of 0.05 mm

### 3. Validation

To validate the presented results the SSPV processes four 3D scans produced with a partly simulated photogrammetry-based system as described in section 2.7. Figure 22 visualizes these 3D scans. The four chosen quality parameters in Metashape – lowest, low, medium and high – correspond per definition in section 2.1 to four 3D scanning systems with an increasing sensor size. As a smaller sensor leads to less pixels per detail the resolution and accuracy and also the point density increases from lowest to high.

Table 1 confirms this prediction. Noticeable is the difference between the two values of the DHD.

Table 1: The results of the validation in terms of resolution and accuracy

Scaled top views of the center of the reproduced Spatial stars	lowest	low	medium	high
	$r = 6975 \text{ mm}$ $r = 14225 \text{ mm}$	$r = 2625 \text{ mm}$ $r = 445 \text{ mm}$	$r = 105 \text{ mm}$ $r = 155 \text{ mm}$	$r = 0.475 \text{ mm}$ $r = 0.6 \text{ mm}$
DHD (see 2.9.2) (solid)	3.36 dhd/cm	10.73 dhd/cm	30.80 dhd/cm	79.58 dhd/cm
SFR 10% (see 2.4) (dashed)	6.82 dhd/cm	18.02 dhd/cm	44.42 dhd/cm	95.49 dhd/cm
median accuracy	0.24 mm	0.07 mm	0.02 mm	0.02 mm

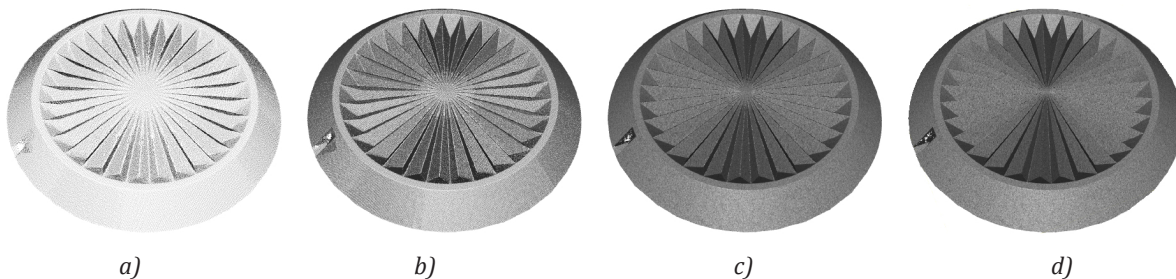


Figure 22: Four partly simulated 3D scans of the Spatial star corresponding to the quality parameters in Metashape: lowest (a), low (b), medium (c) and high (d)

The visualizations in the first row show that the DHD value for the 10 % contrast in the SFR is perceptually more accurate than the DHD value determined as shown in section 2.9.2. The condition to reproduce the correct number of elements seems to be too strict.

Medium and high have the same median accuracy. By comparing the respective accuracy UMR this result is plausible (Figures 23 and 24). Visually the majority of the values for high is around  $0.35 \times NTE$ . While medium has a higher amount of non-tolerable errors, it also has a higher amount of values around  $0.25 \times NTE$ .

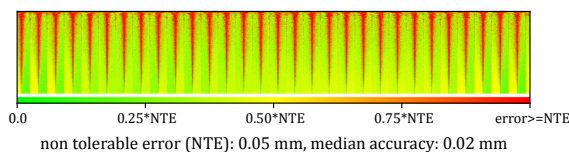


Figure 23: The accuracy UMR for high

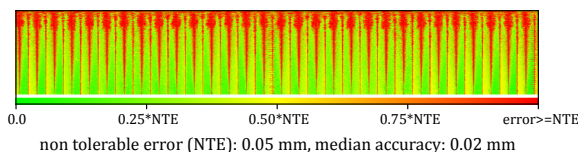


Figure 24: The accuracy UMR for medium

With the decreasing resolution the SFRs of the 3D scan decrease as well (Figure 25). Thus, the high SFR lies completely above the medium SFR, while the medium SFR lies completely above the low SFR which lies completely above the lowest SFR. Noticeable is the characteristic of the SFRs. First the negative slope increases and then turns into a linear negative slope. After the linear decreasing the SFR starts to fluctuate.

Another critical factor is the discretization step as it controls the restructuring of the data. Figure 26 shows the medium SFR for several discretization steps. A larger discretization step results in an increased percentage of the reproduced height. The reason for this is the interpolation. For example, a first point with maximum height lies on radius 0.049 mm. To its left lies a second point with the same height on radius 0.035 mm.

A third point with minimal height lies in between those points on radius 0.029 mm. A discretization step of 0.06 mm shifts all these points to the same radius. The reproduced height is 100 %. A discretization step of 0.03 mm shifts the first and second point to radius 0.06 mm and the third point to radius 0.03 mm. For both radii the reproduced height would be 0 %.

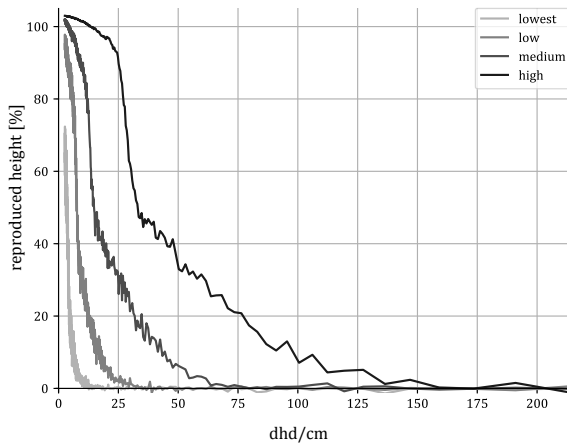


Figure 25: The SFRs of the four partly simulated 3D scans with decreasing resolution and the same discretization step of 0.025 mm

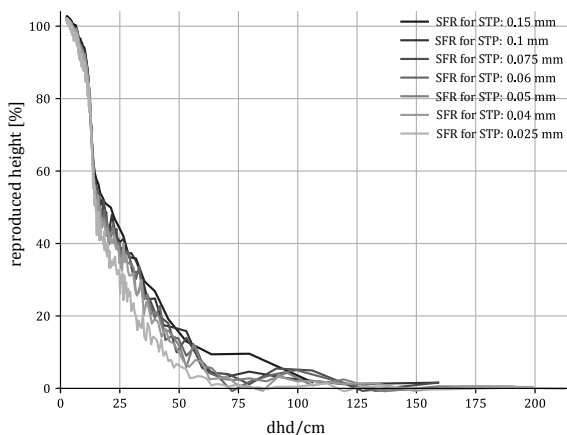


Figure 26: The medium SFR for different discretization steps

#### 4. Discussion and conclusion

This paper has two results. The first result is the Spatial star, a digital testing element to provide the accuracy, resolution and SFR. The second result is the method to restructure a 3D scan of the Spatial star to ensure comparability and to gather and process all required information to determine the accuracy, resolution and SFR. The digital Spatial star therefore allows to determine this information from 3D scans of the Spatial star. The SSPV on the other hand determines the accuracy,

resolution and SFR from an 3D scan of the Spatial star. Therefore, the digital Spatial star in combination with the methods proposed with SSPV built the foundation to implement the workflows shown in the introduction (Figure 1).

The validation shows that the main principle is working. But it also reveals two major issues that need further work. The first one is the influence of the discretization step in combination with the interpolation on the UMR. At the moment only UMRs with the same discretization step are comparable. The optimal discretization step would avoid empty cells in the UMR and therefore minimize the necessity of interpolation. Accordingly, the density of the point cloud defines the optimal discretization step. To get around this issue the processing of triangle meshes will be implemented as the next step.

The second issue is the strict determination of the value of DHD. The DHD value for 10 % reproduced height of the SFR seems to be a good alternative. Further investigations have to proof that this alternative can be transferred to the Spatial star. In respect to the discretization step issue the extracted DHD value needs a visual verification.

With the digital Spatial star this paper introduces a fundamental test element. Further works have to deal with the implementation of the processes required to use the Spatial star in real world scenarios.

One possible implementation could be a workflow to test 3D scanning algorithms or even slicer software for 3D printers. These two testing scenarios can completely be done with the digital Spatial star as no physical object is required. The advantage is the lack of any production uncertainty. In fact, the combination of the partly simulated 3D scans shown in section 2.7 and the validation in section 3 can easily be modified to compare different photogrammetry software.

Another implementation could deal with the testing of 3D printing systems. Here a system under test consists of the slicer software and the 3D printer itself. While the slicer software processes the digital Spatial star into G-code, the 3D printer prints out a physical copy of the Spatial star. The critical part is the re-digitizing of the physical copy as a 3D scanning system depending on its resolution capacity distorts the physical copy by itself.

A good first step would be to use a 3D scanning system with a higher resolution capacity. This raises the question mentioned in the introduction. To what degree the resolution capacity of a 3D scanning system has to be beyond the resolution capacity of the system under test?

Another question is, if the operating principle would work with 3D printers. Figure 27 shows a 3D print-out of the Spatial star described in section 2.7 that looks promising. However real scientific testing has to follow.



Figure 27: A 3D print of the Spatial star (performed by unfurther specified 3D printer)

The implementation of a workflow to test 3D scanning systems would be the most complex task. The problem

here is that the required physical copy of the Spatial star has to have a high degree of detail to be compatible with a wide range of 3D scanning systems. The resolution capacity of the production system has to be at least beyond the resolution capacity of the system under test.

The problem is getting more complex if it comes to creating a digital reference from the physical copy. Here the resolution capacity of the used 3D scanning system has to be beyond the resolution capacity of the production system used. This, from the present point of view, limits the usage of the Spatial star for very detailed 3D scanning systems as the production of the physical copy will be very difficult as well as the creation of the reference. These limits also have to be characterized.

In conclusion, this paper lays the foundation to test several 3D scanning and printing systems. But a lot of work has to be done to implement, characterize and optimize the required processes.

## References

- Agisoft, 2021a, *Metashape standard edition (1.7.3)*. [computer program] Agisoft Limited Liability Company. Available at: <<https://www.agisoft.com/downloads/installer/>> [Accessed 1 June 2021].
- Agisoft, 2021b, *Agisoft Metashape user manual: standard edition, Version 1.7*. [pdf] Agisoft Limited Liability Company. Available at: <[https://www.agisoft.com/pdf/metashape\\_1.7\\_en.pdf](https://www.agisoft.com/pdf/metashape_1.7_en.pdf)> [Accessed 11 October 2021].
- Blender Online Community, 2021. *Blender – a 3D modelling and rendering package (2.92.0)*. [computer program] Stichting Blender Foundation, Amsterdam. Available at: <<http://www.blender.org>> [Accessed 1 June 2021].
- Birch, G.C. and Griffin, J.C., 2015. Sinusoidal Siemens star spatial frequency response measurement errors due to misidentified target centers. *Optical Engineering*, 54(7): 74104. <https://doi.org/10.1117/1.OE.54.7.074104>.
- Brünger, J., Koch, R., Pears, N., Liu, Y., and Rosin, P.L., 2020. Introduction. In: Y. Liu, N. Pears, P.L. Rosin and P. Huber, eds. *3D imaging, analysis and applications*. 2<sup>nd</sup> ed. Cham: Springer International Publishing. Ch. 1.4, pp. 12–17. <https://doi.org/10.1007/978-3-030-44070-1>.
- Canon Deutschland GmbH, 2021. *Canon EOS 750D: Technische Daten*. [online] Available at: <[https://www.canon.de/for\\_home/product\\_finder/cameras/digital\\_slr/eos\\_750d/specifications.html](https://www.canon.de/for_home/product_finder/cameras/digital_slr/eos_750d/specifications.html)> [Accessed 11 October 2021].
- CloudCompare, 2021. *CloudCompare (2.11 Alpha)*. [computer program] Available at: <<http://www.cloudcompare.org/>> [Accessed 11 October 2021].
- Drouin, M.-A. and Beraldin, J.-A., 2020. Active triangulation 3D imaging systems for industrial inspection. In: Y. Liu, N. Pears, P.L. Rosin and P. Huber, eds. *3D imaging, analysis and applications*. 2<sup>nd</sup> ed. Cham: Springer International Publishing. Ch. 3, pp. 109–165. <https://doi.org/10.1007/978-3-030-44070-1>.
- Goesele, M., Fuchs, C., and Seidel, H., 2003. Accuracy of 3D range scanners by measurement of the slanted edge modulation transfer function. In: *Fourth International Conference on 3-D Digital Imaging and Modeling: Proceedings*. Banff, AB, Canada, 6–10 October 2003. IEEE, pp. 37–44. <https://www.doi.org/10.1109/IM.2003.1240230>.
- Guidi, G. and Frischer, B.D., 2020. 3D digitization of cultural heritage. In: Y. Liu, N. Pears, P.L. Rosin and P. Huber, eds. *3D imaging, analysis and applications*. 2<sup>nd</sup> ed. Cham: Springer International Publishing. Ch.13.2.1, pp. 631–697. <https://doi.org/10.1007/978-3-030-44070-1>.
- Harris, C.R., Millman, K.J., van der Walt, S.J., Gommers, R., Virtanen, P., Cournapeau, D., Wieser, E., Taylor, J., Berg, S., Smith, N.J., Kern, R., Picus, M., Hoyer, S., van Kerkwijk, M.H., Brett, M., Haldane, A., Del Río, J.F., Wiebe, M., Peterson, P., Gérard-Marchant, P., Sheppard, K., Reddy, T., Weckesser, W., Abbasi, H., Gohlke, C. and Oliphant, T.E., 2020. Array programming with NumPy. *Nature*, 585, pp. 357–362. <https://www.doi.org/10.1038/s41586-020-2649-2>.
- Harvey, P., 2021. *ExifTool (12.32)*. [computer program] Available at: <<https://exiftool.org/>> [Accessed 01 June 2021].
- Hunter, J.D., 2007. Matplotlib: a 2D graphics environment. *Computing in Science & Engineering*, 9(3), pp. 90–95. <https://www.doi.org/10.1109/MCSE.2007.55>.
- International Organization for Standardization, 2017. *ISO 12233:2017(en) Photography – Electronic still picture imaging – Resolution and spatial frequency responses*. Geneva: ISO.

- Kai, C.C., Jacob, G.G.K. and Mei, T., 1997. Interface between CAD and rapid prototyping systems. Part 1: a study of existing interfaces. *The International Journal of Advanced Manufacturing Technology*, 13(8), pp. 566–570. <https://doi.org/10.1007/BF01176300>.
- Kintel, M., 2021. *OpenSCAD (2021.01)*. [computer program] Available at: <<https://openscad.org/>> [Accessed 01 June 2021].
- Loebich, C., Wueller, D., Kligen, B. and Jaeger, A., 2007. Digital camera resolution measurement using sinusoidal Siemens stars. In: *Proceedings SPIE 6502, Electronic Imaging 2007, Digital Photography III*. San Jose, CA, USA, 20 February 2007. SPIE. <https://doi.org/10.1117/12.703817>.
- Masaoka, K., 2018. Accuracy and precision of edge-based modulation transfer function measurement for sampled imaging systems. *IEEE Access*, 6, pp. 41079–41086. <https://doi.org/10.1109/ACCESS.2018.2856742>.
- McKinney, W., 2010. Data structures for statistical computing in Python. In: S. van der Walt and J. Millman, eds. *Proceedings of the 9<sup>th</sup> Python in Science Conference*. Austin, TX, USA, 28 June – 3 July 2010. SciPy, pp. 56–61. <https://www.doi.org/10.25080/Majora-92bf1922-00a>.
- Se, S. and Pears, N., 2020. Passive 3D imaging. In: Y. Liu, N. Pears, P.L. Rosin and P. Huber, eds. *3D imaging, analysis and applications*. 2<sup>nd</sup> ed. Cham: Springer International Publishing. Ch. 2.2.1, pp. 39–107. <https://doi.org/10.1007/978-3-030-44070-1>.
- Virtanen, P., Gommers, R., Oliphant, T.E., Haberland, M., Reddy, T., Cournapeau, D., Burovski, E., Peterson, P., Weckesser, W., Bright, J., van der Walt, S.J., Brett, M., Wilson, J., Millman, K.J., Mayorov, N., Nelson, A.R.J., Jones, E., Kern, R., Larson, E., Carey, C.J., Polat, İ., Feng, Y., Moore, E.W., VanderPlas, J., Laxalde, D., Perktold, J., Cimrman, R., Henriksen, I., Quintero, E.A., Harris, C.R., Archibald, A.M., Ribeiro, A.H., Pedregosa, F., van Mulbregt, P. and SciPy 1.0 Contributors, 2020. SciPy 1.0: fundamental algorithms for scientific computing in Python. *Nature methods*, 17(3), pp. 261–272. <https://www.doi.org/10.1038/s41592-019-0686-2>.
- Zhou, Q-Y., Park, J. and Koltun, V., 2018. Open3D: a modern library for 3D data processing. *arXiv* [online] Available at: <<http://arxiv.org/pdf/1801.09847v1>> [Accessed 01 June 2021].

